Arg97 at the Heme-Distal Side of the Isolated Heme-Bound PAS Domain of a Heme-Based Oxygen Sensor from *Escherichia coli* (*Ec* DOS) Plays Critical Roles in Autoxidation and Binding to Gases, Particularly O_2[†]

Yukako Ishitsuka, Yasuyuki Araki, Atsunari Tanaka, Jotaro Igarashi, Osamu Ito, and Toru Shimizu*

Institute of Multidisciplinary Research for Advanced Materials, Tohoku University, Sendai 980-8577, Japan

Received February 12, 2008; Revised Manuscript Received May 23, 2008

ABSTRACT: The catalytic activity of heme-regulated phosphodiesterase from *Escherichia coli* (*Ec* DOS) on cyclic di-GMP is markedly enhanced upon binding of gas molecules, such as O_2 and CO, to the heme iron complex in the sensor domain. Arg97 interacts directly with O_2 bound to Fe(II) heme in the crystal structure of the isolated heme-bound sensor domain with the PAS structure (*Ec* DOS-PAS) and may thus be critical in ligand recognition. To establish the specific role of Arg97, we generated Arg97Ala, Arg97Glu, and Arg97Ile mutant *Ec* DOS-PAS proteins and examined binding to O_2, CO, and cyanide, as well as redox potentials. The autoxidation rates of the Arg97Ala and Arg97Glu mutant proteins were up to 2000-fold higher, while the O_2 dissociation rate constant for dissociation from the Fe(II)−O_2 heme complex of the Arg97Ile mutant was 100-fold higher than that of the wild-type protein. In contrast, the redox potential values of the mutant proteins were only slightly different from that of the wild type (within 10 mV). Accordingly, we propose that Arg97 plays critical roles in recognition of the O_2 molecule and redox switching by stabilizing the Fe(II)−O_2 complex, thereby anchoring O_2 to the heme iron and lowering the autoxidation rate to prevent formation of Fe(III) hemin species not regulated by gas molecules. Arg97 mutations significantly influenced interactions with the internal ligand Met95, during CO binding to the Fe(II) complex. Moreover, the binding behavior of cyanide to the Fe(III) complexes of the Arg mutant proteins was similar to that of O_2, which is evident from the K_d values, suggestive of electrostatic interactions between cyanide and Arg97.

Heme-regulated phosphodiesterase from *Escherichia coli* (*Ec* DOS)[1] is composed of a heme iron-binding sensor domain at the N-terminus and a catalytic domain at the C-terminus (*1*). *Ec* DOS catalyzes the conversion of cyclic di-GMP to linear di-GMP, and its activity is regulated by gas binding to the heme iron complex in the sensor domain (*1, 2*). Specifically, binding of O_2, CO, or NO to Fe(II) heme in the sensor domain markedly enhances phosphodiesterase activity toward cyclic di-GMP by up to 8-fold (*2*). These characteristics induced by gas molecules are inconsistent with those of other well-known gas-responsive heme sensor proteins, such as FixL, CooA, and soluble guanylate cyclase, which strictly recognize O_2, CO, and NO, respectively, to regulate catalysis or transcription (*3, 4*). *Ec* DOS is an unprecedented novel gas sensor enzyme that does not differentiate among these gas molecules for catalytic regulation. Since the CO and NO concentrations in cells are very low (nanomolar), it is likely that *Ec* DOS is predominantly an oxygen sensor enzyme whereby catalysis is regulated in response to the micromolar O_2 level. However, the mechanisms by which external ligands, such as O_2, bind to the heme iron, the specific residues forming the ligand access channel, and ligand recognition techniques of the enzyme are currently unclear. The molecular mechanism of O_2 recognition by *Ec* DOS that facilitates intramolecular signal transduction from the sensor domain to the catalytic domain requires further elucidation.

The crystal structures of Fe(III), Fe(II), and Fe(II)−O_2 complexes of the isolated heme-bound sensor domain with the PAS structure of *Ec* DOS (*Ec* DOS-PAS) have been reported previously (*5, 6*). The side chain of Arg97 interacts directly with the O_2 molecule bound to iron in the Fe(II)−O_2 complex, whereas Met95 is the axial ligand for the Fe(II) complex (Figure 1). However, the structure of the distal side of the Fe(III) complex was not determined due to the excess flexibility of the protein. Arg97 is the only residue that serves as a direct O_2 binding site on the distal side and may thus have a key function in the recognition of external ligands for catalytic regulation. In this study, we analyze ligand binding to the heme iron, autoxidation, and redox potentials of Arg97 mutant proteins, with the aim of establishing the specific role of this residue in ligand association or recognition.

[†] This work was in part supported by a Grant-in-Aid and by the Special Education and Research Expenses from the Ministry of Education, Culture, Sports, Science, and Technology of Japan to T.S.

* To whom correspondence should be addressed. Telephone: +81-22-217-5604, 5605. Fax: +81-22-217-5604, 5390. E-mail: shimizu@tagen.tohoku.ac.jp.

[1] Abbreviations: *Ec* DOS, heme-regulated phosphodiesterase from *E. coli*; *Ec* DOS-PAS, isolated heme-bound sensor domain with the PAS structure of *Ec* DOS; Fe(III) complex, Fe(III) hemin or Fe(III) protoporphyrin IX complex; Fe(II) complex, Fe(II) protoporphyrin IX complex; FixL, heme-binding oxygen sensor kinase; CooA, CO-sensing transcriptional factor from the photosynthetic bacterium *Rhodospirillum rubrum*; SHG, second harmonic generation; OPA, optical parametric amplifier; MOS, metal oxide semiconductor; Nd:YAG, neodymium-doped yttrium aluminum garnet; PDB, Protein Data Bank.

10.1021/bi800248c CCC: $40.75
Published on Web 08/02/2008

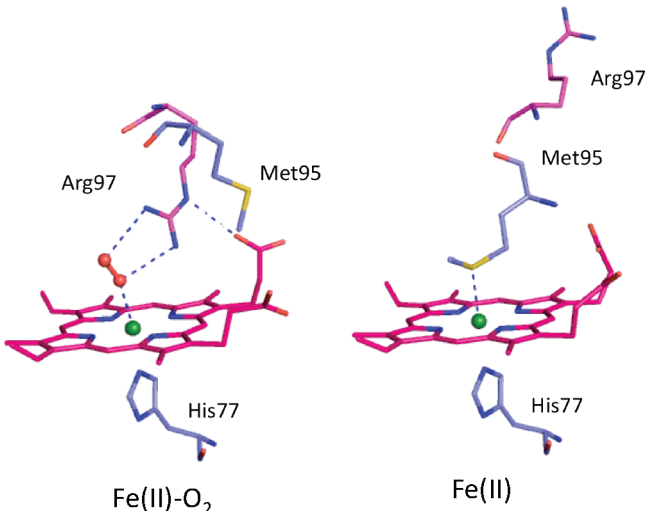

FIGURE 1: Crystal structures of the Fe(II)−O_2 (left, PDB entry 1VB6) and Fe(II) (right, PDB entry 1V9Z) complexes of *Ec* DOS-PAS.

We generated Arg97Ala, Arg97Glu, and Arg97Ile mutant *Ec* DOS-PAS proteins and examined various physicochemical characteristics. The autoxidation rates of the three Arg97 mutants were substantially higher than that of the wild-type protein. Moreover, the rate of dissociation of O_2 from the Arg97Ile mutant was significantly faster than that of the wild-type protein. Our results strongly suggest that Arg97 plays critical roles in O_2 recognition by *Ec* DOS in terms of autoxidation and O_2 dissociation. In addition, the data imply that the Arg97 mutation significantly affected the mode of binding of the internal ligand, Met95, to Fe(II), during the CO rebinding process, as suggested by the Met95 rebinding behavior of the mutants observed during the CO rebinding process. Also, interactions of cyanide with the Fe(III) complex of the Arg97 mutant proteins appeared to be similar to those of O_2 with the Fe(II) complex in terms of K_d values, implying electrostatic interactions between cyanide and Arg97. Previous reports show that Met95 mutations markedly enhance the binding of axial ligands (*9–11*). Here, we compare the effects of Arg97 mutations on physicochemical characteristics of the enzyme with those of Met95 mutations and another heme-based oxygen sensor enzyme, FixL (*3*).

EXPERIMENTAL PROCEDURES

Materials. All chemical reagents were purchased from Wako Pure Chemicals (Osaka, Japan). Reagents were of the highest commercial grade available and used without further purification. The QuikChange site-directed mutagenesis kit was from Stratagene (La Jolla, CA). Oligonucleotides employed for plasmid construction and site-directed mutagenesis were obtained from Nihon Gene Research Laboratory (Sendai, Japan).

Construction of Expression Plasmids. Cloning of *Ec* DOS-PAS and construction of the expression plasmid, pET28a(+), were performed, as described previously (*7–11*).

Site-Directed Mutagenesis. Arg97 mutants were generated using the QuikChange site-directed mutagenesis kit with pET28a(+) containing wild-type *Ec* DOS-PAS as a template and the following primers: 5′-gttgaggggatgagtGCGgagctgcagctggag-3′ (forward) and 5′-ctccagctgcagctcCGCactcatcccctcaac-3′ (reverse) for Arg97Ala, 5′-gttgaggggatgagtGAAgagctgcagctggag-3′ (forward) and 5′-ctccagctgcagctcTTCactcatcccctcaac-3′ (reverse) for Arg97Glu, and 5′-gttgaggggatgagtATTgagctgcagctggag-3′ (forward) and 5′-ctccagctgcagctcAATactcatcccctcaac-3′ (reverse) for Arg97Ile. All constructs were confirmed by DNA sequencing.

Protein Expression and Purification. Protein expression in *E. coli* and purification procedures were conducted as described previously, with slight modifications (*7–11*). Briefly, wild-type and mutant *Ec* DOS-PAS proteins were overexpressed in *E. coli* BL21(DE3) using the pET28a(+) plasmid containing an N-terminal six-His tag and thrombin cleavage site. A single colony was inoculated in 50 mL of Luria-Bertani (LB) medium containing 20 μg/mL kanamycin and 0.5% glucose and shaken overnight at 200 rpm and 37 °C. The cultured medium was added to 1 L of terrific broth (TB) containing 20 mg/mL kanamycin, followed by shaking for 4 h at 120 rpm and 37 °C. After the medium had been cooled to 20 °C, δ-aminolevulinic acid was added to adjust to the final concentration 0.45 mM, and the mixture was incubated with shaking for an additional 20 h. *E. coli* cells were harvested by centrifugation for 10 min at 5000*g* and 4 °C and stored at −80 °C.

Protein purification procedures were performed on ice or at 4 °C. *E. coli* cells frozen at −80 °C were suspended in 50 mM potassium phosphate buffer (pH 7.5) containing 20 mM imidazole, 150 mM NaCl, 5% glycerol, 1 mM phenylmethanesulfonyl fluoride (buffer A), and 0.1 mg/mL lysozyme. The solution was sonicated and centrifuged at 100000*g* for 30 min. Supernatant fractions were applied to a nickel−nitrilotriacetic acid−agarose column. *Ec* DOS-PAS fractions were eluted with a linear gradient from 20 to 300 mM imidazole in buffer A. The solution containing *Ec* DOS-PAS was dialyzed against 20 mM Tris-HCl (pH 8.0) with 5% glycerol (buffer B). Thrombin protease (Wako Pure Chemicals) (1 unit/mg of protein) was added to cleave the His tag. Subsequently, the sample solution was applied to a nickel−nitrilotriacetic acid−agarose column, and His tag-free *Ec* DOS-PAS eluted in the flow-through fractions using buffer B. *Ec* DOS-PAS fractions were subjected to DEAE column chromatography and eluted with a linear gradient from 0 to 1 M NaCl in buffer B. After dialysis of proteins against buffer B, purified *Ec* DOS-PAS was concentrated with Centriprep (Millipore, Billerica, MA) or Amicon Ultra (Millipore) concentrators. Purified proteins were >95% homogeneous, as confirmed with sodium dodecyl sulfate−polyacrylamide gel electrophoresis. Samples were stored at −20 °C in 40% glycerol (*2*).

Optical Absorption Spectroscopy. Static spectral data were recorded using UV-1600PC and UV-2500PC (Shimadzu, Kyoto, Japan) spectrophotometers under aerobic conditions. The heme of *Ec* DOS-PAS proteins was reduced using small quantities of sodium dithionite in 50 mM Tris-HCl (pH 8.0) and 50 mM NaCl. The Fe(II) complex was prepared in N_2-saturated buffer. The Fe(II) heme−CO complex was prepared in CO-saturated buffer. Gas-saturated solutions were obtained by bubbling the buffer with the appropriate gas for at least 30 min.

Stopped-Flow Spectroscopy. Kinetic studies of association of the external axial ligands with the wild-type and Arg97 mutant proteins were conducted according to previous reports (*9, 13*). We used the RSP-1000 stopped-flow mixing apparatus (Unisoku, Osaka, Japan). All measurements were

performed at 25 °C using a temperature controller. The reaction buffer consisted of 50 mM Tris-HCl (pH 8.0) and 50 mM NaCl.

Redox Potentials. Redox potential values were obtained essentially according to previous reports (*7, 11, 12*). Anaerobic spectral experiments were performed in a glovebox using a Shimadzu UV-160A spectrometer and an ORION Research (Tokyo, Japan) model 701 digital pH meter equipped with a TOA (Tokyo, Japan) saturated calomel microelectrode (SCE). Spectral experiments were performed with 10 μM protein in 50 mM phosphate buffer (pH 7.0) and 50 mM NaCl at 15 °C. 2,3,5,6-Tetramethylphenylenediamine (276 mV, 10 mM), *N*-ethylphenazonium ethosulfate (55 mV, 10 mM), and 2-hydroxy-1,4-naphthaquinone (−152 mV, 10 mM) were added to samples as mediators before titration.

Laser Flash Photolysis. Picosecond and nanosecond transient absorption spectra were recorded using the pump-and-probe method with a Ti:sapphire regenerative amplifier seeded by SHG of an Er-doped fiber laser (Clark-MXR CPA-2001 plus, 1 kHz, fwhm of 150 fs). A white continuum pulse used as a monitoring light was generated by focusing the fundamental of the amplifier on a rotating H_2O cell. Samples were excited using the SHG (388 nm) of fundamental or output of OPA (Clark-MXR vis-OPA, 560 nm). The monitoring light transmitted through the sample in a rotating cell with a path length of 2 mm was distinguished with a dual MOS detector (Hamamatsu Photonics, C6140) equipped with a polychromator. Approximately 60% of bound CO was dissociated with the pump-and-probe apparatus. Note that this value does not represent the quantum yield for the CO dissociation but depends on the cross section between the probe light and laser light. Proteins [25 μM in 50 mM Tris-HCl (pH 8.0) and 50 mM NaCl] were utilized at room temperature.

Laser flash photolysis experiments in the microsecond and millisecond domains for the Fe(II)−CO complexes were performed at 25 °C in the 1 cm cell used for optical absorption spectroscopy. The protein concentration employed was 15 μM in 50 mM Tris-HCl (pH 8.0) and 50 mM NaCl. We used the second harmonic light (532 nm) of a Nd:YAG laser (Continuum, Surelite II-10) with fundamental radiation at 1064 nm. The monitoring light was produced using a 150 W xenon lamp. The laser peak power was 30 mJ with a pulse width of 6 ns (a repetition rate of 2 Hz) from a xenon lamp, and the light intensity was reduced by up to 80% at a wavelength of <380 nm. Details of the equipment have been described previously (*9, 13*). Approximately 70% of bound CO was dissociated upon laser photolysis. Note that this value does not represent the quantum yield for the CO dissociation, but depends on the cross section between the probe light and laser light. To assess changes from the six-coordinate His77−Fe(II)−CO complex to the five-coordinate His77−Fe(II) complex, recovery of *Ec* DOS-PAS-CO was monitored at 434−440 nm with continuous light from a xenon lamp using an oscilloscope (Hewlett-Packard, Infinium). We additionally monitored the absorption decrease at 437 nm, but changes from the Fe(II)−His77 complex to the His77−Fe(II)−Met95 complex were not observed due to the proximity of the isosbestic point. All rate constants were calculated using Igor Pro (WaveMetrics). Experiments were performed at least twice for each complex. Data obtained from five or more points could be reproduced within a 20% margin of experimental error. Transients of bimolecular association of CO and Fe(II) heme in *Ec* DOS-PAS or Met95 coordination were recorded as the average of at least 10 measurements. The flash photolysis time course between 0 and 400 μs monitored at 434−440 nm for the wild-type, Arg97Ala, and Arg97Ile mutant proteins was composed of three phases (~80 μs, ~800 μs, and ~400 ms) and analyzed using the equation $\Delta\mathrm{Abs}(t) = Ae^{-k_1 t} + Be^{-k_2 t} + Ce^{-k_3 t}$, where ΔAbs represents the total intensity change at a certain time, t, after flash, A, B, and C are initial intensities for each phase, and k_1, k_2, and k_3 are the rate constants for Met95 rebinding and CO recombination. In Table 4, Met95 ligation (first phase), fast phase (second phase), and slow phase (third phase) correspond to rate constants k_1, k_2, and k_3, respectively.

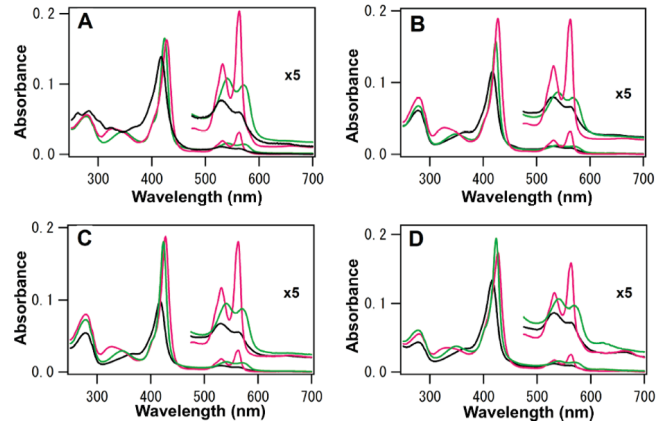

FIGURE 2: Optical absorption spectra of the Fe(II) (pink line), Fe(II)−CO (green line), and Fe(III) (black line) complexes of wild-type and Arg97 mutant proteins of the isolated heme-bound domain (*Ec* DOS-PAS): (A) wild type (5 μM), (B) Arg97Ala (5 μM), (C) Arg97Glu (5 μM), and (D) Arg97Ile (5 μM).

Cyanide Binding. To estimate the ligand association rates, spectral changes in the heme of *Ec* DOS-PAS were monitored after the addition of cyanide in 50 mM Tris-HCl (pH 7.5) (*10, 12, 14*). We assume that the cyanide−*Ec* DOS-PAS complex is generated via a pseudo-first-order reaction ($k_{obs} = k_{on}[\mathrm{KCN}] + k_{off}$). As the actual time course for the change in heme absorbance of WT and Arg97 mutant proteins is monophasic, the observed pseudo-first-order rate constant (k_{obs}) was obtained by fitting to an exponential function, $A_{total}(t) = Ae^{-k_{obs}t}$. Plots of k_{obs} versus [KCN] were linear (Figure 8C), leading to the calculation of k_{on} values from the equation $k_{obs} = k_{on}[\mathrm{KCN}] + k_{off}$.

Cyanide dissociation experiments were performed by diluting 30−50 μM cyanide-bound heme protein solutions into 1 mL of buffer. Prior to the reaction, excess cyanide was separated from the cyanide−*Ec* DOS-PAS complex using a Sephadex G-25 desalting chromatography column (GE Healthcare, Little Chalf-ont, U.K.). All dissociation reactions followed first-order kinetics. Accordingly, dissociation rates were calculated by curve fitting to a single-exponential function.

RESULTS

Optical Absorption Spectra of the Arg97 Mutant Ec DOS-PAS Proteins. Figure 2 depicts the optical absorption spectra of the Fe(II), Fe(II)−CO, and Fe(III) complexes of wild-type (A), Arg97Ala (B), Arg97Glu (C), and Arg97Ile (D)

Table 1: Optical Absorption Spectral Maxima (nanometers) of the Fe(II), Fe(II)−O_2, Fe(II)−CO, Fe(III), and Fe(III)−CN Complexes of Wild-Type and Arg97 Mutant *Ec* DOS-PAS Proteins

	Fe(II)			Fe(II)−O_2			Fe(II)−CO			Fe(III)			Fe(III)−CN	
Ec DOS-PAS	S^a	β	α	S^a	β	α	S^a	β	α	S^a	β	α	S^a	visible
wild type	428	532	563	417	542	579	424	540	572	417	529	561	420	542
Arg97Ala	428	532	563	nd[b]			424	542	568	418	531	563	423	542
Arg97Glu	428	532	563	nd[b]			424	541	570	418	531	560	421	541
Arg97Ile	427	533	563	417	541	579	424	541	569	416	532	563	422	539

[a] Soret band. [b] Not determined due to rapid autoxidation rate constants.

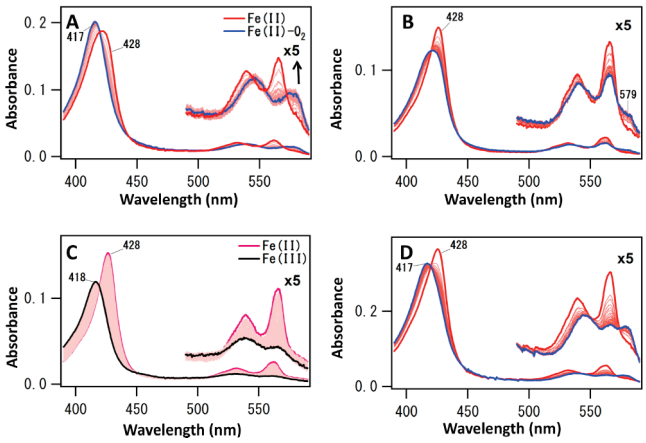

FIGURE 3: Spectral changes of the Fe(II) complexes (pink line) of wild-type (A), Arg97Ala (B), Arg97Glu (C), and Arg97Ile (D) proteins accompanied by mixing with O_2-saturated buffer on the stopped-flow spectrometer. Each line was obtained at a 10 ms interval after mixing for wild-type, Arg97Ala, and Arg97Ile proteins, while for Arg97Glu, each line was obtained at a 40 ms interval. The wild-type protein formed a stable Fe(II)−O_2 complex (blue line). However, Fe(II)−O_2 complexes of the Arg97Glu mutants were very unstable upon mixing of the protein solution with O_2-saturated buffer on the stopped-flow spectrometer, and thus, only the Fe(III) complex (black line) was observed. In contrast, for the Arg97Ala and Arg97Ile mutants, the Fe(II)−O_2 complex was partially and transiently observed under similar conditions on the stopped-flow spectrometer.

Ec DOS-PAS proteins. The spectra of all the *Ec* DOS-PAS mutant complexes are typical of six-coordinate low-spin heme proteins, similar to that of wild-type *Ec* DOS-PAS (Table 1). Therefore, it appears that the heme environment structure, including the heme coordination state (six-coordinate low-spin complex), is not altered by the Arg mutations. The Arg mutant proteins generated in this study are worthy of further investigation.

O_2 Association and Dissociation Properties of Arg97 Mutants of Ec DOS-PAS. The Fe(II)−O_2 complex of the wild-type protein was sufficiently stable for analysis of the optical absorption spectrum (Table 1 and Figure 3A) (*7, 9*). Formation of the Fe(II)−O_2 complex was evident from the increased absorption peaks at 417, 542, and 579 nm approximately 10 ms after mixing the Fe(II) complex with the O_2-saturated buffer in a stopped-flow spectrometer (Figure 3A). The association of O_2 with the Fe(II) complex of *Ec* DOS-PAS occurred over two phases. Pseudo-first-order rate constants were evaluated, since both phases were O_2 concentration-dependent (Table 2) (*13*). The rate constant for dissociation of O_2 from the wild-type protein was obtained by mixing the Fe(II)−O_2 complex- and CO-saturated solutions since dissociation of O_2 from the Fe(II) complex is accompanied by rapid association of CO to the Fe(II) complex (Figure 2S of the Supporting Information) (*9, 23*). Both association and dissociation rate constants of O_2 for the wild-type protein were comparable to previously reported values (Table 2).

For the Arg97Ala mutant, the small absorption peak at 579 nm of the Fe(II)−O_2 complex was observed approximately 500 ms after mixing with O_2-saturated buffer. However, this band quickly disappeared due to rapid autoxidation to the Fe(III) complex (Figure 3B). This finding indicates that the O_2 molecule binds transiently to heme in the mutant protein. It was not feasible to evaluate the exact O_2 concentration-dependent association and dissociation rate constants for the Arg97Ala mutant protein. However, the apparent O_2 association rate constant was estimated to be 76×10^{-3} μM^{-1} s^{-1} by monitoring absorption at 426 nm at a concentration of 650 μM O_2 (Table 2).

For the Arg97Glu mutant, only rapid successive reaction from the Fe(II) to Fe(III) complexes was observed after mixing the Fe(II) complex solution with O_2-saturated buffer (Figure 3C). Once the Fe(II)−O_2 complex was formed, rapid autoxidation was initiated, and complex detection was thus not feasible. A combination of two or three factors, specifically, slow O_2 binding, fast O_2 dissociation, and fast autoxidation of the mutant protein, allowed the detection of only continuous transitions from the Fe(II) to Fe(III) complexes, even using a stopped-flow spectrometer.

For the Arg97Ile mutant, the Fe(II)−O_2 complex was partially observed when the Fe(II) complex solution was mixed with O_2-saturated buffer in the stopped-flow spectrometer (Figure 3D). The spectrum obtained at 500 ms displayed a majority fraction of the Fe(II)−O_2 complex along with a minor proportion of the Fe(II) complex. However, a more stable Fe(II)−O_2 complex was observed from spectra obtained on a conventional absorption spectrometer when the Fe(II) complex solution was diluted into O_2-saturated buffer (Figure 4A), although the autoxidation rate constant of the Arg97Ile mutant was significantly faster than that of the wild-type protein (Figure 4B and Table 3). In the stopped-flow spectrometer, the O_2 concentration (1.3 mM) of O_2-saturated buffer is diluted to half by mixing with protein solution, whereas on the conventional spectrometer, the O_2 concentration remains at 1.3 mM. Therefore, the O_2 molecule would associate with the Fe(II) complex more quickly when the protein is diluted into O_2-saturated buffer on a conventional spectrometer than under conditions where the protein solution is mixed with O_2-saturated buffer on a stopped-flow spectrometer. Thus, formation of the Fe(II)−O_2 complex governs rapid autoxidation, leaving the stable Fe(II)−O_2 complex on the conventional spectrometer for the Arg97Ile mutant. The O_2 association rate for the Arg97Ile mutant was composed of two phases. Both phases were O_2 concentration-dependent, and the second-order rate constants were deter-

Table 2: O_2 Association and Dissociation Rate Constants of Arg97 and Other Mutant *Ec* DOS-PAS Proteins[a]

protein	O_2 association: fast phase, k_{on} ($\times 10^{-3}$ μM^{-1} s^{-1})	O_2 association: slow phase, k_{on} ($\times 10^{-3}$ μM^{-1} s^{-1})	O_2 dissociation (s^{-1})	K_d (μM)	ref
wild type	37	3.0	0.79	21	this work
	81	8.3			*13*
	31		0.61	20	*9*
Arg97Ala	76[b]		nd		this work
Arg97Glu	nd		nd		this work
Arg97Ile	155	14	78	500	this work
Met95Ala	>1000		0.73	<0.73	*9*
Met95His	>1000		0.79	<0.79	*9*
Met95Ile	160		0.22	1.4	*23*
Met95Leu	>1000		0.45	<0.45	*9*
Leu99Phe	75				*13*
Leu99Thr	49	6.8			*13*
Leu115Thr	55	7.2			*13*

[a] Arg97, Met95, Leu99, and Leu115 are located on the heme-distal side. [b] While it was unfeasible to obtain O_2 concentration dependencies of the O_2 association rate, the apparent O_2 association rate constant was evaluated by monitoring absorption at 426 nm at an O_2 concentration of 650 μM. The value obtained by monitoring absorption at 579 nm was essentially similar to that described here.

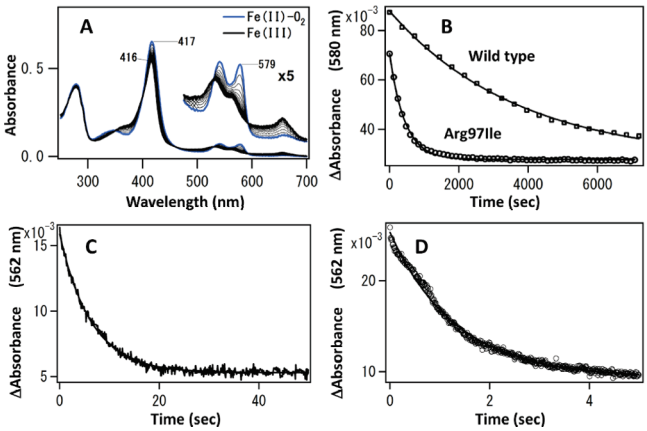

FIGURE 4: Spectral changes of the Arg97Ile mutant (A) and time-dependent spectral intensity changes monitored at 580 nm of the wild-type (□) and Arg97Ile mutant (○) proteins (B) for autoxidation and at 562 nm of the Arg97Ala (C) and Arg97Glu (D) mutants, accompanied by binding of O_2 to the Fe(II) heme complex. Arrows in panel A indicate spectral changes from the Fe(II)−O_2 (blue line) to Fe(III) (black line) complexes. Data depicted in panel B were obtained after the Fe(II) complexes were diluted into O_2-saturated buffer on the conventional spectrometer, while data depicted in panels C and D were obtained after mixing Fe(II) complexes with O_2-saturated buffer on the stopped-flow spectrometer. The final O_2 concentrations were 520 and 650 μM for the Arg97Ala and Arg97Glu mutants, respectively. A small band at approximately 660 nm appeared for the mutant proteins after the Fe(II) heme complex was diluted into O_2-saturated buffer. This may represent a heme-modified species with O_2, which is yet to be identified.

mined to be 155 and 14 × 10^{-3} μM^{-1} s^{-1}, respectively (Table 2 and Figure 1S of the Supporting Information). In contrast, the O_2 dissociation rate constant for the Arg97Ile mutant was 78 s^{-1}, 100-fold higher than that of the wild-type protein (Table 2 and Figure 2S of the Supporting Information). The equilibrium dissociation constant (K_d) for dissociation of O_2 from the Arg97Ile protein evaluated from the dissociation and association rate constants was 500 μM, which is also significantly larger than that of the wild-type protein [21 μM (Table 2)]. This high K_d value is consistent with spectral behavior in which the stable Fe(II)−O_2 complex is observed at an O_2 concentration of 1.3 mM on the conventional spectrometer, but not at 650 μM O_2 on the stopped-flow spectrometer.

Table 3: Autoxidation Rates and Redox Potentials (millivolts vs SHE) of Arg97 and Other Mutant *Ec* DOS-PAS Proteins[a]

protein	autoxidation rate (min^{-1})	redox potential: reductive	redox potential: oxidative	ref
wild type	0.0050 with air-saturated buffer	45 (n = 1.00)	38 (n = 1.03)	this work
	0.022 with O_2-saturated buffer			this work
	0.0058	24	53	*9*, *13*
Arg97Ala	>9.5[b]	43 (n = 0.96)	29 (n = 1.13)	this work
Arg97Glu	>46[b]	40 (n = 1.00)	27 (n = 1.13)	this work
Arg97Ile	0.16 with O_2-saturated buffer	49 (n = 1.13)	*c*	this work
Met95Ala	0.0013	−26		*9*, *11*
Met95His	0.016	−122		*9*, *11*
Met95Leu	0.0017	−1		*9*, *11*
Leu99Thr	0.049	23	20	*13*
Leu99Phe	0.37	24	38	*13*
Leull5Thr	0.065	35	25	*13*
Leull5Phe	0.33	nd	nd	*13*
Asp40Ala	0.051	95		*12*
Asp40Asn	0.033	114		*12*

[a] O_2-saturated buffer was used to form the Fe(II)−O_2 complexes. Arg97, Met95, Leu99, and Leu115 are located on the heme-distal side, whereas Asp40 is located at the heme proximal side. [b] Apparent autoxidation rate constants were obtained with a stopped-flow spectrometer. Final O_2 concentrations of the Arg97Ala and Arg97Glu mutants were 520 and 650 μM, respectively. Since the Fe(II)−O_2 complex was not observed for Arg97Ala and Arg97Glu mutants, we state the minimal values. [c] Oxidative titration did not stop at the initial spectrum, suggestive of protein structural changes. Thus, we have not cited the oxidative value for the Arg97Ile mutant.

Autoxidation of Arg97 Mutants of Ec DOS-PAS. The autoxidation rate constant of the wild-type protein was very low (0.005 min^{-1}) upon dilution with air-saturated buffer (0.022 min^{-1}) or O_2-saturated buffer (Table 3). In contrast, the autoxidation rate constants of the Arg97Ala and Arg97Glu mutant proteins were very high, specifically, more than 9.5 and 46 min^{-1}, respectively (Table 3 and Figure 4C,D). The autoxidation rate constant of the Arg97Ile mutant was 0.16 min^{-1} with O_2-saturated buffer (Figure 4B−D and Table 3). Consequently, the order of autoxidation rate constants for the proteins is as follows: Arg97Glu > Arg97Ala > Arg97Ile > wild type. Notably, the autoxidation rate constants of the Arg97Ala and Arg97Glu mutants are the highest among those of the *Ec* DOS-PAS proteins hitherto reported (Table 3).

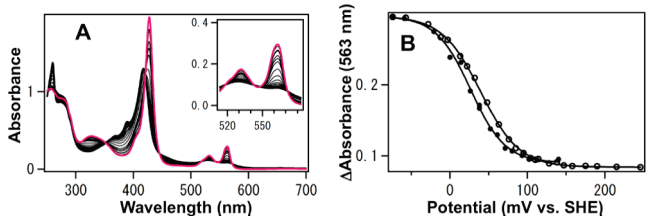

FIGURE 5: (A) Spectral changes of the Arg97Glu mutant protein upon reduction with sodium dithionite. The arrows designate alterations in the spectrum of the Fe(III) complex (black line) to the Fe(II) complex (red line). (B) Electrochemical reductive (○) and oxidative (●) titrations of the Arg97Glu mutant of *Ec* DOS-PAS. Experimental data are fitted to the calculated lines. See Experimental Procedures for details.

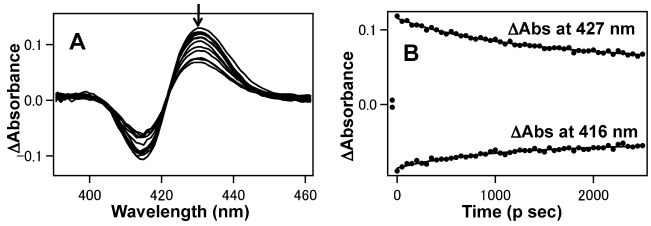

FIGURE 6: Laser flash photolysis of the Fe(II)−CO complex of wild-type *Ec* DOS-PAS in the picosecond and nanosecond domains. Difference spectra (A) and difference spectral changes (B) monitored at 427 nm (top) and 416 nm (bottom) are shown. No significant differences were evident between the wild-type and Arg97 mutant proteins.

Redox Potentials. The autoxidation rate constants of the Arg97 mutants were significantly higher than that of the wild-type protein. In general, the autoxidation rate reflects several factors, such as the electrostatic environment of the heme plane, ionic interactions of the distal oxygen atom of O_2 bound to the Fe(II) complex, or redox potentials of the heme iron complex (*15*). Accordingly, we measured the redox potentials of the Arg97 mutant proteins (Figure 5). Interestingly, the redox potential values of the three Arg97 mutant proteins were only slightly different (within 10 mV vs SHE) from those of the wild-type protein (Table 3). However, redox potential values of other mutant *Ec* DOS-PAS proteins at the heme-distal or -proximal sides were distinct from those of the wild type (more than 30 mV vs SHE) (Table 3).

Association of CO with Arg97 Mutant Proteins. To establish the role of Arg97 in ligand recognition, we examined CO binding kinetics and compared these with O_2 interactions. Initially, we observed spectral changes in the picosecond and nanosecond domains for the wild-type and Arg97 mutant *Ec* DOS-PAS proteins. Approximately 40% of the dissociated CO molecules were re-bound in the picosecond domain for the wild-type and Arg97 mutant proteins (Table 4). Transient spectra obtained after dissociation of CO from *Ec* DOS-PAS are depicted in Figure 6. No significant evolution on the time scale (up to a few hundred picoseconds) was observed, while a marked decrease in the signal was evident on the nanosecond time scale. The half-amplitude of our data as a function of time fit to a single-exponential decay with a time constant of 2.5 ns, similar to previous reports (*27*). The first-order rate constant, evaluated as 5.7×10^8 s^{-1} for the wild-type protein, was not dependent on the CO concentration (Table 4). No significant differences in time-dependent spectral changes within the nanosecond time domain were evident between the wild-type and Arg97 mutant proteins (Table 4).

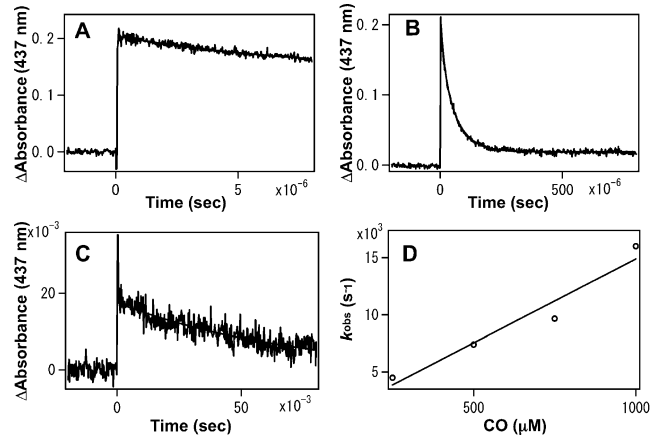

FIGURE 7: Laser flash photolysis of the Fe(II)−CO complex of the Arg97Ala mutant of *Ec* DOS-PAS. The flash photolysis time course of the Arg97Ala mutant monitored at 437 nm was composed of three phases, specifically, first (~80 μs) (A), second (~800 μs) (B), and third (~400 ms) (C), and plotted directly from digitalized data. Both the second (B) and third (C) phases of the rate constants for CO binding to the Arg97Ala mutant were dependent on the CO concentration. The pseudo-first-order rate constants for CO binding to the five-coordinate Fe(II) protein (B) were obtained by least-squares fitting of flash photolysis data (D). See Table 4 for details.

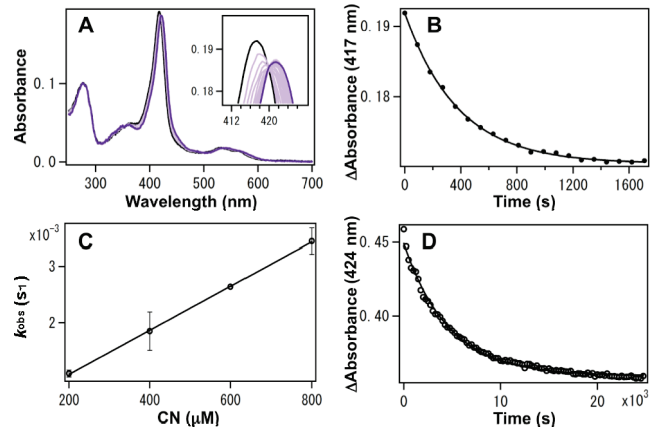

FIGURE 8: (A) Optical absorption spectral changes for the Arg97Ala mutant of *Ec* DOS-PAS (2.0 μM) caused by binding cyanide (KCN, 0.6 mM) in 50 mM Tris-HCl (pH 7.5). The Soret region was expanded, since spectral changes were small. Each spectrum was obtained 90 s after addition of the cyanide solution. Data for the Fe(III) complex are shown with a black line, whereas data for the Fe(III)−CN complex are represented with a cyan line. (B) Absorption intensity changes monitored at 417 nm vs time after addition of cyanide. Filled circles are experimental data, while the solid line is theoretical. (C) Dependence of the first-order rate constants for cyanide binding to *Ec* DOS-PAS on cyanide concentration. (D) Absorption intensity changes monitored at 424 nm vs time after dilution of cyanide-bound Arg97Ala into the buffer solution. Empty circles are experimental points, whereas the line is theoretical.

Wild-type and Arg97 mutant proteins were subjected to flash photolysis in the microsecond domain for analyzing CO binding to the Fe(II) complex (Figure 7). The flash photolysis time course between 0 and 400 μs, monitored at 434−440 nm, was composed of three phases, specifically, ~80 μs, ~800 μs, and ~400 ms (Table 4). The spectral change in the first phase (within a time range of less than 80 μs) of the wild-type protein was 3.0×10^4 s^{-1} and independent of the CO concentration (Table 4). Thus, spectral changes in this time domain reflect coordination of Met95 with the Fe(II) complex (Table 4) (*13, 23*). For Arg97Ala,

Table 4: CO Association Rate Constants for Arg97 and Other Mutants of *Ec* DOS-PAS[a]

Ec DOS-PAS	geminate[b] $\times 10^8$ s^{-1}	Met95 ligation[c] ($\times 10^4$ s^{-1}), first phase	fast phase k_{on} (μM^{-1} s^{-1}), second phase	slow phase k_{on} (μM^{-1} s^{-1}), third phase	ref
wild type	5.7 (44%)	3.0 (43%)[d]	2.1	0.028 (13%)	this work
			7.8		*9*
Arg97Ala	9.9 (45%)	3.5 (50%)[d]	15	0.0074 (4%)	this work
Arg97Glu	9.0 (51%)	5.0, 0.39[e] (20%, 15%)		0.17 (15%)	this work
Arg97Ile	6.4 (36%)	(<1%)	11 (61%)	0.086 (3%)	this work
Met95Ala			9.3		*9*
Met95His			6.2		*9*
Met95Ile			1.1		*23*
Met95Leu			3.4		*9*
Leu99Phe		5.7		0.044	*13*
Leu99Thr		6.3		0.029	*13*
Leull5Thr		6.3		0.041	

[a] Fractions of spectral changes of the proteins corresponding to each rate constant are specified in parentheses. [b] Geminate CO rebinding to the Fe(II) complex is CO concentration-independent. [c] CO concentration dependence was not observed. Thus, we assume that spectral changes are due to ligation of Met95 to the Fe(II) complex, as suggested previously (*13, 23*). [d] Fractions of the first and second phases were not separated for the wild-type and Arg97Ala proteins. [e] For the Arg97Glu mutant, CO binding with a time domain of 10^4 s^{-1} was composed of two components. The two components (5.0 and 0.39 $\times$ 10^4 s^{-1}) were CO concentration-independent.

no significant differences in rates were observed within this time domain in comparison to that of the wild type (Table 4). For Arg97Ile, the time domain of the first phase was so minor that we could not obtain the rate constant. The smaller fraction of the first phase (Met95 ligation) seen with the Arg97Ile mutant (compared with the wild type) may be associated with the smaller fraction of the third phase (the CO concentration-dependent slow phase) concomitantly present, because the third phase should reflect CO binding to the five-coordinate complex associated with Met95 ligand dissociation, as discussed below. However, CO binding to the Arg97Glu protein was distinct from those of the wild-type, Arg97Ala, and Arg97Ile proteins in that the domain was composed of only the first and third phases. The first phase had two components (5.0 and 0.39 $\times$ 10^4 s^{-1}), which were independent of the CO concentration (Table 4). Because the two components of the first phase were not dependent on CO concentration, it appears reasonable to suggest that for the Arg97Glu mutant, Met ligation occurs in a manner distinct from that in the wild-type protein and other Arg97 mutants.

The flash photolysis time courses at ~800 μs (second phase) and ~400 ms (third phase) for CO binding to the Fe(II) wild-type, Arg97Ala, and Arg97Ile proteins were dependent on the CO concentration (Figure 7). The second phase reflects CO binding to the five-coordinate heme iron complex, whereas the third phase represents CO binding to the Met95-ligated six-coordinate heme iron complex. Accordingly, the second-order rate constants were evaluated from the pseudo-first-order rate constants, as summarized in Table 4. Significant increases in the rate constants of the second phase were observed for the Arg97Ala and Arg97Ile mutant proteins (from 2.1 up to 15 $\times$ 10^{-3} μM^{-1} s^{-1}), compared with that of the wild-type protein. The Arg97Glu mutant protein displayed an unusual first phase and lacked a second phase. This finding may be explained by marked alterations in the heme-distal structure induced upon mutation from Arg to Glu, including the Met ligation mode and CO access channel.

The fractions of the photoinduced spectral changes are summarized in parentheses in Table 4. Fractions of geminate rebinding were not significantly different between wild-type and Arg97 mutant proteins. Individual fractions were not separately evaluated for the first and second phases of wild-type and Arg97Ala proteins, and thus, total fractions are described. Due to the unusual distal structures induced by the Arg97Glu mutation, we failed to detect the second phase. For the Arg97Ile mutant, the minor fraction of the first phase is associated with the small fraction of the third phase, suggesting that the Ile residue interacts with Met95. We rationalize this in the Discussion.

Table 5: Cyanide Association and Dissociation Rate Constants for Arg97 and Other Mutant *Ec* DOS-PAS Proteins

Ec DOS-PAS	association k_{on} ($\times 10^{-4}$ μM^{-1} s^{-1})	dissociation k_{off} ($\times 10^{-4}$ s^{-1})	K_d (μM)	ref
wild type	0.42	1.2	2.9	this work
	0.45	4.1	9.1	*10*, *12*
	0.14	0.62	44	*23*
Arg97Ala	0.039	2.0	51	this work
Arg97Glu	0.016	2.5	160	this work
Arg97Ile	0.14	5.3	38	this work
Met95Ala	5	$\ll$0.1	$\ll$0.2	*10*
Met95His	0.026	0.93	35	*10*
Met95Ile	0.71	0.38	0.5	*23*
Met95Leu	3.8	$\ll$0.1	$\ll$0.2	*10*
Asp40Ala	0.65			*12*
Asp40Asn	0.73			*12*

Association of Cyanide with Arg97 Mutants of Ec DOS-PAS. Cyanide binding studies provide valuable structural and ionic information about the heme-distal side of heme proteins and the stable Fe(II)$-O_2$ complex analogue. Fe(III)$-$cyanide complexes of the wild-type and Arg97 mutant *Ec* DOS-PAS proteins exhibited a Soret peak at approximately 421 nm and visible absorption at approximately 540 nm (Table 1 and Figure 2S of the Supporting Information). No significant spectral differences in the Fe(III)$-$CN complexes were evident between wild-type and Arg97 mutant proteins. However, cyanide association rate constants of the Arg97Ala (0.039 $\times$ 10^{-4} μM^{-1} s^{-1}) and Arg97Glu (0.016 $\times$ 10^{-4} μM^{-1} s^{-1}) mutant proteins were markedly lower than that (0.42 $\times$ 10^{-4} μM^{-1} s^{-1}) of the wild-type protein (Table 5 and Figure 8). These results are inconsistent with those of CO binding,

whereby the rates of association of CO with the Arg97 mutants are significantly higher than that of the wild-type protein (Table 4).

Rate constants for dissociation of cyanide from Arg97 mutant proteins were similar to that of the wild-type protein (Table 5). These findings are at variance with the association rate constants obtained for cyanide with the Arg97 mutant proteins. Consequently, the equilibrium dissociation constant values were substantially higher than that of the wild-type protein, suggesting that the mutations markedly hinder binding of cyanide to the Fe(III) complex in *Ec* DOS-PAS.

DISCUSSION

O_2 Association and Dissociation Properties of Arg97 Mutant Proteins. Upon O_2 binding to the Fe(II) complex, the NH1 and NH2 atoms of Arg97 moved 13.5 and 11.6 Å, respectively, whereas the Cα atom only shifted 1.7 Å. This significant shift of atoms led to rearrangement of the heme environment. The side chain of Arg97 interacts with the O_2 molecule bound to the Fe(II) complex in *Ec* DOS-PAS (Figure 1). Mutation of Arg97 led to a loss of hydrogen bonds between the Arg side chain and O_2 molecule bound to the heme iron. Therefore, it is reasonable to assume that the O_2 binding behavior of Arg97 mutant proteins is distinct from that of the wild-type protein, since the mutations eliminate the anchor to hook the O_2 molecule on the heme plane. Introduction of a hydrophobic residue into the distal side in the Arg97Ala and Arg97Ile mutants may add to the hydrophobic character at the O_2 access channel, thus slightly facilitating binding of the O_2 molecule, which is also assumed to have a hydrophobic character. The loss of the bond between Arg97 and O_2 released locking of O_2 to the heme iron and substantially enhanced the O_2 dissociation rate of the Arg97Ile mutant (100-fold). As a result, the equilibrium dissociation constant of O_2 for the Arg97Ile mutant was 24-fold higher than that of the wild-type protein (Table 2). It is possible that the O_2 dissociation rate constants of the Arg97Ala and Arg97Glu mutants are higher than that of the wild-type protein. However, these rate constants were not evaluated, since we could not detect a distinct Fe(II)−O_2 complex for the mutants. Our results collectively suggest that Arg97 plays a critical role in fixing the O_2 molecule to the heme iron to prevent the rapid O_2 dissociation observed with the Arg97Ile mutant proteins. Further studies are required to unequivocally address this issue.

Conversely, substantial enhancement of the O_2 association rate constants is reported for the Met95 mutant proteins (Table 2) (*9, 23*). This finding may be explained by the assumption that the axial ligand, the side chain of Met95, hampers direct binding of the external ligand to the heme iron and is removed upon mutation of this residue.

A low-intensity band at approximately 660 nm appeared in spectra derived from mutant proteins after the Fe(II) heme complex was diluted into O_2-saturated buffer (Figure 4). This band might arise from the interaction of high-valence iron−oxo intermediates with the porphyrin macrocycle. Probably, Arg97 mutant proteins have inappropriate heme-distal structures that allow the generation of byproducts such as reactive oxygen species, with consequent modification of the porphyrin macrocycle, whereas the wild-type protein has a heme-distal structure optimal for oxygen sensing; therefore, no byproducts are generated. However, the addition of catalase or superoxide dismutase to the mutant protein did not influence the intensity of the band near 660 nm (data not shown). Further studies to address the issue remain to be conducted.

Autoxidation Rate Constants of Arg97 Mutant Proteins. The autoxidation rate of the heme iron complex is associated with several factors (*15*). The electrostatic characteristics or polarities of the environment of the heme iron complex and O_2 molecule bound to the heme iron, redox potentials of iron, electrostatic characteristics of porphyrin, and other factors contribute to autoxidation of heme iron in the protein (*9, 15*). Since the side chain of Arg97 interacts with the O_2 molecule bound to the heme iron in *Ec* DOS-PAS (Figure 1), interactions between Arg97 and O_2 should play critical roles in stabilizing the O_2−heme complex and lowering the autoxidation rate constant.

The autoxidation rate constant of the Arg97Glu mutant was significantly higher than that of the Arg97Ala mutant (Figure 4 and Table 3). Possibly, introduction of Glu containing a side chain of the opposite ionic character at position 97 substantially alters the ionic characteristics of the heme-distal side, leading to the marked enhancement of autoxidation. The cyanide association rate constant of the Arg97Glu mutant was, however, smaller than that of the Arg97Ala mutant, and substantially less than that of the wild-type protein (Table 5), suggesting that the anionic side chain of Glu97 in the Arg97Glu mutant is located so close to the cyanide access channel of the Fe(III) complex that the two anionic groups exercise mutual electrostatic repulsion. Therefore, our observations on the autoxidation and cyanide binding of the Arg97Glu mutants are internally consistent.

The Fe(II)−O_2 complex of the Arg97Ile mutant protein was unstable and undetectable, even after the heme solution had been mixed with O_2-saturated buffer (final O_2 concentration of 650 μM) on the stopped-flow spectrometer. However, when the Fe(II) complex of the Arg97Ile mutant protein was diluted into O_2-saturated (1.3 mM) buffer, the stable Fe(II)−O_2 complex was observed, even on a conventional absorption spectrometer. This finding may be attributed to the high K_d value of the Arg97Ile mutant protein for O_2. The O_2 association rate constant for binding of the Fe(II) complex to Arg97Ile is rapid, up to 155×10^{-3} μM^{-1} s^{-1}. Thus, at sufficiently high O_2 concentrations (1.3 mM), the Fe(II)−O_2 complex forms quickly. Complex stability, in turn, governs the autoxidation rate (0.16 min^{-1}), allowing us to observe the Fe(II)−O_2 complex, even with a conventional spectrometer.

The O_2 concentration in bacterial cells is on the order of micromolar, whereas the NO or CO concentration should be nanomolar or lower (*16*). Thus, the O_2 gas is the most likely candidate as the first signal for regulation of the *Ec* DOS enzyme, although NO and CO gases also enhance catalysis (*2*). The Fe(III) complex in *Ec* DOS does not receive this gas molecule as an axial ligand, and thus, the binding of O_2 to the Fe(III) complex in *Ec* DOS does not occur. The Fe(III) complex of *Ec* DOS has essentially very low catalytic activity. Therefore, prevention of the redox change from Fe(II) to Fe(III) complexes may additionally be very important for catalytic regulation, since *Ec* DOS is regulated in response to O_2 gas. On the basis of the results, we suggest that Arg97 plays a critical role in the recognition

of O_2, particularly via facilitating O_2 binding and avoidance of rapid autoxidation. The rigid structure of the FG loop of the Fe(II) complex distal side, in contrast to the flexible structure of the Fe(III) complex distal side, may additionally act to ensure that Arg97 works as part of the oxygen sensor mechanism of *Ec* DOS (*1, 5*).

Association of CO with Arg97 Mutant Proteins. Geminate CO recombination rate constants of Arg97 mutant proteins were not significantly different from those of the wild-type protein (Table 4). Ultrafast CO binding on the nanosecond time scale upon photolysis reflects the proximity of CO to the heme plane, since CO does not move away from the heme plane within such short time periods. Arg97 is located a slight distance from the heme plane. Consequently, Arg97 mutations do not affect the CO binding rate on the nanosecond time scale.

Ultrafast recombination studies in the picosecond time domain of *Ec* DOS associated with internal ligand binding have been reported previously (*26–28*). It was suggested that Met95 is rebound to the Fe(II) complex in the 100 μs domain after flash photolysis of the Fe(II)−CO complex (*27*). In this study, we observe only a minor fraction of Met ligation in the Arg97Ile mutant protein (Table 4), suggesting that introduction of Ile at position 97 induces substantial alterations in Met ligation behavior. Moreover, unusual Met95 ligation was observed for the Arg97Glu mutant in terms of the presence of two components in the first phase (Table 4), suggesting that the substitution leads to two binding modes.

The Arg97Ala and Arg97Ile mutations induced an increase in the CO concentration-dependent association rate constants corresponding to CO binding to the five-coordinate heme (second phase) up to 7-fold (Table 4). Loss of specific interactions between Arg97 and the heme 7-propionate in the mutant proteins may contribute to an increase in the CO binding rate, as suggested by resonance Raman spectroscopic findings (*30*) that will be discussed below.

For the six-coordinate low-spin complex with His/Met ligation, CO binds to the heme with a rate that is limited by the off rate of Met95. The third phase of CO association (as reflected in the appropriate rate constant) should reflect this, and the third phase was indeed altered in Arg97 mutant proteins (Table 4). Moreover, the smaller fraction of the third phase (compared with that of the wild type) for Arg97Ile appears to be associated with a smaller fraction of the first phase (Met95 ligation). Resonance Raman spectroscopic findings also suggested that mutations at Arg97 significantly influenced the transient binding of Met95 to heme upon photodissociation of CO (*30*); these data are in good agreement with the findings presented here. We therefore conclude that Arg97 mutations alter the mode of binding of the Met95 residue to the Fe(II) complex.

Our findings collectively suggest that Met95 and Arg97 on the flexible FG loop interact during the ligand switching process that is critical in intramolecular signal transduction. Resonance Raman spectroscopic data on Arg97 mutant proteins additionally suggest that cleavage of the hydrogen bond between the 7-propionate of the heme and formation of a new hydrogen bond between the 7-propionate and Met95 are accompanied by a structural change upon photodissociation of CO (*30*).

Quantum Yield of CO Photodissociation of the Arg97 Mutant Ec DOS-PAS Proteins. The quantum yield of CO photodissociation reflects the probability of escape of CO from the heme iron and is useful in evaluating the degree of proximity of heme iron and the heme-distal amino acid residues (*32*). For example, mutations of the axial ligand, Met80, of cytochrome *c* (*32–34*), or of the heme-distal amino acids of myoglobin (*35*), significantly change the quantum yield of CO photodissociation. Also, the presence of substrate significantly changes the quantum yields of photodissociation of CO from cytochrome P450 enzymes (*36, 37*). The quantum yield of the wild-type *Ec* DOS-PAS−CO complex relative to that of the myoglobin−CO complex (defined as unity) was approximately 0.9. Mutations at Arg97 did not significantly change the quantum yield (within experimental error), as measured by CO binding kinetic values, suggesting that Arg97 does not significantly influence the direct CO escape channel. Further studies should focus on CO or O_2 escape probabilities associated with the gas sensor function of *Ec* DOS.

Cyanide Binding to Arg97 Mutant Proteins. The pK_a value of HCN is 9.14. Thus, the actual concentration of cyanide at pH 7.5 should be considerably lower than that of added KCN. A recent comprehensive study of cyanide binding to myoglobin (*31*) indicated that the major determinants of cyanide affinity for the heme pocket are the ease of water displacement from the ferric ion atom, the acid dissociation constant of HCN inside the heme pocket, and steric hindrance and electrostatic interactions at the sixth coordination position. Because the Fe(III) form of *Ec* DOS-PAS has a hydroxide anion (or a water molecule) at the sixth position, similar factors, including overall polarity, accessibility, and the size of the distal pocket, should contribute to the affinity of the heme pocket cyanide for the wild-type and Arg97 mutant proteins of *Ec* DOS-PAS. However, we could not determine the heme-distal structure of the Fe(III) complex of *Ec* DOS-PAS because of the flexibility of the distal main and side chains, and we thus cannot offer a detailed, results-based, discussion of the cyanide binding structure of this study.

The rate constants for association of cyanide with the Arg97 mutants were lower than that of the wild-type protein, while the dissociation rate constants were slightly higher (Table 5). As a result, the equilibrium dissociation constants of the Arg97 mutants were up to 55-fold higher than that of the wild-type protein, suggesting that the residue at position 97 enhances the affinity of cyanide for wild-type *Ec* DOS and the Fe(III)−CN complex stability in terms of the K_d value, similar to O_2 binding. This finding is reminiscent of another heme-based oxygen sensor enzyme, FixL (*3, 22*; discussed later), whereby the function and structure of the Fe(III)−CN complex of FixL are similar to those of the Fe(II)−O_2 complex (*29*). For BjFixL, the Fe(III)−CN complex is the analogue of the Fe(II)−O_2 complex. Specifically, Arg220 corresponding to Arg97 in *Ec* DOS interacts electrostatically with CN bound to the Fe(III) complex in BjFixL. In view of these cyanide binding data, we propose that Arg97 of *Ec* DOS interacts electrostatically with cyanide, like BjFixL (*29*).

Association of cyanide with the Fe(III) complex is quite slow. Arg97 mutations further weaken cyanide binding and destabilize the Fe(III)−CN complex. These results are inconsistent with Met95 mutation data. Specifically, Met95 mutations (except Met95His) substantially enhance the

cyanide association rate constant and drastically decrease the dissociation rate constants, ultimately leading to reduced equilibrium dissociation constants (Table 5) (*10*). Therefore, it seems unlikely that Met95 in the wild-type protein functions in stabilizing the Fe(III)−CN complex. The X-ray crystal structure of the Fe(III) complex of *Ec* DOS-PAS disclosed that the axial ligand on the distal side should be water or hydroxide anion, but the distal structure could not be determined, probably due to the flexibility of the distal region in the Fe(III) complex. However, given that Met95 mutations dramatically affect the cyanide binding rate, it is possible that Met95 is located in the proximity of the heme plane, even in the Fe(III) complex, but does not contribute to stabilization of the Fe(III)−CN complex. We speculate that Arg97 is located near the cyanide molecule and thus mutations at this site significantly increase the K_d value for cyanide, similar to O_2 binding. Cyanide may electrostatically bind Arg97, similar to interactions between O_2 and Arg97.

Comparison with Arg Residues at the Heme-Distal Side of the Heme-Based Oxygen Sensor Enzyme, FixL. FixL is another heme-based oxygen sensor enzyme with a heme-bound PAS domain (*3*). The structures and functions of the Fe(II)−O_2 and Fe(III)−CN complexes of the isolated heme domains of FixL are similar (*3, 22*). Arg residues at the heme-distal side of FixL are important for catalytic regulation of FixL in response to association of O_2 with the Fe(II) complex. X-ray crystal structures of the Fe(II) complexes of FixL revealed substantial structural changes at the heme-distal side upon binding of O_2 to the Fe(II) complex. Specifically, (1) the distal Arg (position 220 in BjFixL) side chain forms hydrogen bonds with heme propionate group 7 when the Fe(II) complex of FixL is unliganded, i.e., the "catalytic on state", and (2) the Arg 220 guanidino group forms a hydrogen bond with O_2 for the Fe(II)−O_2 complex, i.e., the "catalytic off state" (*22*). Association of O_2 to and dissociation of O_2 from the Fe(II) complex of FixL regulate catalysis. This is possible because the Fe(II) complex is the major stable form, probably due to its very high redox potential value, and its autoxidation is very slow (<0.001 min^{-1}). O_2, CO, and cyanide association rate constants of the Arg mutant proteins were significantly different from those of the wild-type proteins (*14, 17–21*). However, no Arg mutants on the heme-distal side of FixL display fast autoxidation rates, as observed for the Arg97 mutants of *Ec* DOS-PAS. Thus, in this study, we establish a critical role of Arg97 in stabilizing the Fe(II)−O_2 complex as part of the oxygen sensor mechanism. The O_2 sensing and recognition function of Arg97 of *Ec* DOS is probably considerably more essential than that of the corresponding Arg residues of FixL.

Summary. The autoxidation rate constant of *Ec* DOS-PAS is substantially increased by mutation of Arg97, the side chain of which directly interacts with O_2 bound to the Fe(II) complex in the sensor domain. To date, no substantial increases in the autoxidation rate have been reported for distal mutants of other heme-based oxygen sensor proteins. Thus, these marked increases in the autoxidation rate constant induced by mutations at the heme-distal side of *Ec* DOS-PAS are a novel finding. Arg97 may play a critical role in fixing O_2 on the heme iron, forming the stable Fe(II)−O_2 complex, and inhibiting fast autoxidation to ensure effective heme-based oxygen sensor function of *Ec* DOS. Results of the CO binding kinetic study indicate that Met95 and Arg97 on the flexible FG loop critically interact with each other during the ligand switching process, which is important in intramolecular signal transduction for catalysis. Moreover, Arg97 may interact with cyanide in the Fe(III) complex, like the Fe(II)−O_2 complex. Domain−domain interactions (*24*) and involvement of the heme propionic acids in catalysis (*25*) require further investigation to ascertain the molecular mechanism of intramolecular signal transduction of *Ec* DOS.

ACKNOWLEDGMENT

We thank Dr. Miki Matsui-Watanabe for her work at the initial stages of this study.

SUPPORTING INFORMATION AVAILABLE

Determination of the k_{on} value for binding of O_2 to the Arg97Ile mutant protein and of the k_{off} value for dissociation of O_2 from wild-type and Arg97Ile mutant *Ec* DOS-PAS using a stopped-flow spectrometer and optical absorption spectra of Fe(III) and Fe(III)−CN complexes of wild-type, Arg97Ala, Arg97Glu, and Arg97Ile *Ec* DOS-PAS. This material is available free of charge via the Internet at http://pubs.acs.org.

REFERENCES

1. Sasakura, Y., Yoshimura-Suzuki, T., Kurokawa, H., and Shimizu, T. (2006) Structure-function relationships of *Ec* DOS, a heme-regulated phosphodiesterase from *Escherichia coli*. *Acc. Chem. Res. 39*, 37–43.
2. Tanaka, A., Takahashi, H., and Shimizu, T. (2007) Critical Role of the Heme Axial Ligand, Met95, in Locking Catalysis of the Phosphodiesterase from *Escherichia coli* (*Ec* DOS) toward Cyclic di-GMP. *J. Biol. Chem. 282*, 21301–21307.
3. Gilles-Gonzalez, M. A., and Gonzalez, G. (2005) Heme-based sensors: Defining characteristics, recent developments, and regulatory hypothesis. *J. Inorg. Biochem. 99*, 1–22.
4. Uchida, T., and Kitagawa, T. (2005) Mechanism for transduction of the ligand-binding signal in heme-based gas sensory proteins revealed by resonance Raman spectroscopy. *Acc. Chem. Res. 38*, 662–670.
5. Kurokawa, H., Lee, D. S., Watanabe, M., Sagami, I., Mikami, B., Raman, C. S., and Shimizu, T. (2004) A redox-controlled molecular switch revealed by the crystal structure of a bacterial heme PAS sensor. *J. Biol. Chem. 279*, 20186–20193.
6. Park, H., Suquet, C., Satterlee, J. D., and Kang, C. (2004) Insights into signal transduction involving PAS domain oxygen-sensing heme proteins from the X-ray crystal structure of *Escherichia coli* DOS heme domain (Ec DosH). *Biochemistry 43*, 2738–2746.
7. Sasakura, Y., Hirata, S., Sugiyama, S., Suzuki, S., Taguchi, S., Watanabe, M., Matsui, T., Sagami, I., and Shimizu, T. (2002) Characterization of a direct oxygen sensor heme protein from *Escherichia coli*: Kinetics of the heme redox states and mutations at the heme-biniding site on catalysis and structure. *J. Biol. Chem. 277*, 23821–23827.
8. Sato, A., Sasakura, Y., Sugiyama, S., Sagami, I., Shimizu, T., Mizutani, Y., and Kitagawa, T. (2002) Stationary and time-resolved resonance Raman spectra of His77 and Met95 mutants of the isolated heme domain of a direct oxygen sensor from *Escherichia coli*. *J. Biol. Chem. 277*, 32650–32658.
9. Taguchi, S., Matsui, T., Igarashi, J., Sasakura, Y., Araki, Y., Ito, O., Sugiyama, S., Sagami, I., and Shimizu, T. (2004) Binding of oxygen and carbon monoxide to a heme-regulated phosphodiesterase from *Escherichia coli*: Kinetics and infrared spectra of the full-length wild-type enzyme, isolated PAS domain, and Met95 mutants. *J. Biol. Chem. 279*, 3340–3347.
10. Watanabe, M., Matsui, T., Sasakura, Y., Sagami, I., and Shimizu, T. (2002) Unusual cyanide bindings to a heme-regualted phoephodiesterase from *Escherichia coli*: Effect of Met95 mutations. *Biochem. Biophys. Res. Commun. 299*, 169–172.
11. Hirata, S., Matsui, T., Sasakura, Y., Sugiyama, S., Yoshimura, T., Sagami, I., and Shimizu, T. (2003) Characterization of Met95

mutants of a heme-regulated phosphodiesterase from *Escherichia coli*: Optical absorption, magnetic circular dichroism, circular dichroism, and redox potentials. *Eur. J. Biochem. 270*, 4771–4779.
12. Watanabe, M., Kurokawa, H., Yoshimura-Suzuki, T., Sagami, I., and Shimizu, T. (2004) Critical role of Asp40 at the haem proximal side of haem-regulated phosphodiesterase from *Escherichia coli* in redox potential, auto-oxidation and catalytic control. *Eur. J. Biochem. 271*, 3937–3942.
13. Yokota, N., Araki, Y., Kurokawa, H., Ito, O., Igarashi, J., and Shimizu, T. (2006) Critical roles of Leu99 and Leu115 at the heme distal side in auto-oxidation and the redox potential of a heme-regulated phosphodiesterase from *Escherichia coli*. *FEBS J. 273*, 1210–1223.
14. Tanaka, A., Nakamura, H., Shiro, Y., and Fujii, H. (2006) Role of the heme distal residues of FixL in O_2 sensing; A single convergent structure of the heme moiety is relevant to the downregulation of kinase activity. *Biochemistry 45*, 2515–2523.
15. Springer, B. A., Sligar, S. G., Olson, J. S., and Phillips, G. N. (1994) Mechanism of Ligand Recognition in Myoglobin. *Chem. Rev. 94*, 699–714.
16. Huang, S. H., Rio, D. C., and Marletta, M. (2007) Ligand binding and inhibition of an oxygen-sensitive soluble guanylate cyclase, Gly-88E, from *Drosophila*. *Biochemistry 46*, 15115–15122.
17. Jasaitis, A., Hola, K., Bouzhir-Sima, L., Lambry, J. C., Balland, V., Vos, M. H., and Lieb, U. (2006) Role of distal arginine in early sensing intermediates in the heme domain of the oxygen sensor FixL. *Biochemistry 45*, 6018–6026.
18. Balland, V., Bouzhir-Sima, L., Kiger, L., Marden, M. C., Vos, M. H., Liebl, U., and Mattioli, T. A. (2005) Role of arginine 220 in the oxygen sensor FixL from *Bradyrhizobium japonicum*. *J. Biol. Chem. 280*, 15279–15288.
19. Balland, V., Bouzhir-Sima, L., Anxolabéhère-Mallart, E., Boussac, A., Vos, M. H., Lieble, U., and Mattioli, T. A. (2006) Functional implications of the propionate 7-arginine 220 interaction in the FixLH oxygen sensor from *Bradyhizobium japonicum*. *Biochemistry 45*, 2072–2084.
20. Gilles-Gonzalez, M. A., Caceres, A. I., Sousa, E. H. S., Tomchick, D. R., Brautigam, C. A., Gonzalez, C., and Machius, M. (2006) A proximal arginine R206 participates in switching of the *Bradyrhizobium japonicum* FixL oxygen sensor. *J. Mol. Biol. 360*, 80–89.
21. Hiruma, Y., Kikuchi, A., Tanaka, A., Shiro, Y., and Mizutani, Y. (2007) Resonance Raman observation of the structural dynamics of FixL on signal transduction and ligand discrimination. *Biochemistry 46*, 6086–6096.
22. Gong, W., Hao, B., and Chan, M. K. (2000) New mechanistic insights from structural studies of the oxygen-sensing domain of *Bradyrhizobium japonicum* FixL. *Biochemistry 39*, 3955–3962.
23. Gonzalez, G., Dioum, E. M., Bertokucci, C. M., Tomita, T., Ikeda-Saito, M., Cheesman, M. R., Watmough, N. J., and Gilles-Gonzalez, M. A. (2002) Nature of the displaceable heme-axial residue in the *Ec* Dos protein, a heme-based sensor from *Escherichia coli*. *Biochemistry 41*, 8414–8421.
24. Yoshimura, T., Sagami, I., Sasakura, Y., and Shimizu, T. (2003) Relationships between heme incorporation, tetramer formation and catalysis of a heme-regulated phosphodiesterase from *Escherichia coli*: A study of deletion and site-directed mutants. *J. Biol. Chem. 278*, 53105–53111.
25. El-Mashtoly, S. F., Takahashi, H., Shimizu, T., and Kitagawa, T. (2007) Ultraviolet resonance Raman evidence for utilization of the heme 6-propionate hydrogen-bond network in signal transmission from heme to protein in *Ec* DOS Protein. *J. Am. Chem. Soc. 129*, 3556–3563.
26. Yamashita, T., Bouzhir-Sima, L., Lambry, J. C., Liebl, U., and Vos, M. H. (2008) Ligand dynamics and early signaling events in the heme domain of the sensor protein dos from *Escherichia coli*. *J. Biol. Chem. 283*, 2344–2352.
27. Lieb, U., Bouzhir-Sima, L., Kiger, L., Marden, M. C., Lambry, J. C., Négrerie, M., and Vos, M. H. (2003) Ligand binding dynamics to the heme domain of the oxygen sensor dos from *Escherichia coli*. *Biochemistry 42*, 6527–6535.
28. Lieb, U., Bouzhir-Sima, L., Négrerie, M., Martin, J. L., and Vos, M. H. (2002) Ultrafast ligand rebinding in the heme domain of the oxygen sensors FixL and Dos: General regulatory implications for heme-based sensors. *Proc. Natl. Acad. Sci. U.S.A. 99*, 12771–12776.
29. Hao, B., Isaza, C., Joseph Arndt, J., Soltis, M., and Chan, M. K. (2002) Structure-based mechanism of O_2 sensing and ligand discrimination by the FixL heme domain of *Bradyrhizobium japonicum*. *Biochemistry 41*, 12952–12958.
30. El-Mashtoly, S. F., Nakashima, S., Tanaka, A., Shimizu, T., and Kitagawa, T. (2008) Roles of Arg-97 and Phe-113 in regulation of distal ligand binding to heme in the sensor domain of *Ec* DOS protein: Resonance raman and mutation study. *J. Biol. Chem. 283*, 19000–19010.
31. Dou, Y., Olson, J. S., Wilkinson, A. J., and Ikeda-Saito, M. (1996) Mechanism of hydrogen cyanide binding to myoglobin. *Biochemistry 35*, 7107–7113.
32. Brunori, M., Giacometti, G. M., Antonini, E., and Wyman, J. (1973) Heme proteins: Quantum yield determined by the pulse method. *Proc. Natl. Acad. Sci. U.S.A. 70*, 3141–3144.
33. Silkstone, G., Stanway, G., Brzezinsky, P., and Wilson, M. T. (2002) Production and characterization of Met80X mutants of yeast iso-1-cytochrome *c*: Spectral, photochemical and binding studies on ferrous derivatives. *Biophys. Chem. 98*, 65–77.
34. Silkstone, G., Jasaitis, A., Wilson, M. T., and Vos, M. H. (2007) Ligand dynamics in an electron transfer protein: Picosecond geminate recombination of carbon monoxide to heme in mutant forms of cytochrome c. *J. Biol. Chem. 282*, 1638–1649.
35. Carver, T. E., Rohlfs, R. J., Olson, J. S., Gibson, Q. H., Blackmore, R. S., Springer, B. A., and Sligar, S. G. (1990) Analysis of the kinetic barrier for ligand binding to sperm whale myoglobin using site-directed mutagenesis and laser photolysis. *J. Biol. Chem. 265*, 20007–20020.
36. Shimada, H., Iizuka, T., Ueno, R., and Ishimura, Y. (1979) Correlation between the Quantum Yields of Photodissociation and C-O Stretching Frequencies of Carbon Monoxide Hemoproteins. *FEBS Lett. 98*, 290–294.
37. Mitani, F., Iizuka, T., Shimada, H., Ueno, R., and Ishimura, Y. (1985) Flash Photolysis Studies on the CO Complexes of Ferrous Cytochrome $P\text{-}450_{scc}$ and Cytochrome $P\text{-}450_{11b}$: Effects of Steroid Binding on the Photochemical and Ligand Binding Properties. *J. Biol. Chem. 260*, 12042–12048.

BI800248C